Voltage-sensor movements describe slow inactivation of voltage-gated sodium channels I: Wild-type skeletal muscle $Na_V1.4$

Jonathan R. Silva and Steve A.N. Goldstein

Department of Biochemistry, Brandeis University, Waltham, MA 02453

The number of voltage-gated sodium (Na_V) channels available to generate action potentials in muscles and nerves is adjusted over seconds to minutes by prior electrical activity, a process called slow inactivation (SI). The basis for SI is uncertain. Na_V channels have four domains (DI–DIV), each with a voltage sensor that moves in response to depolarizing stimulation over milliseconds to activate the channels. Here, SI of the skeletal muscle channel $Na_V1.4$ is induced by repetitive stimulation and is studied by recording of sodium currents, gating currents, and changes in the fluorescence of probes on each voltage sensor to assess their movements. The magnitude, voltage dependence, and time course of the onset and recovery of SI are observed to correlate with voltage-sensor movements 10,000-fold slower than those associated with activation. The behavior of each voltage sensor is unique. Development of SI over 1–160 s correlates best with slow immobilization of the sensors in DI and DII; DIII tracks the onset of SI with less fidelity. Showing linkage to the sodium conduction pathway, pore block by tetrodotoxin affects both SI and immobilization of all the sensors, with DI and DII significantly suppressed. Recovery from SI correlates best with slow restoration of mobility of the sensor in DIII. The findings suggest that voltage-sensor movements determine SI and thereby mediate Na_V channel availability.

The Journal of General Physiology

INTRODUCTION

Sodium currents through voltage-gated sodium (Na_V) channels activate and inactivate rapidly over several milliseconds. The molecular determinants of these rapid events have been studied extensively. The Na_V channel corpus is a single large subunit with four homologous domains that fold to create a single central ion conduction pore with four nonidentical voltage-sensor domains, each carrying a positively charged S4 span (Fig. 1, A and B) (Catterall et al., 2005). On stimulatory depolarization, the S4 spans are propelled outward by the electric field: the pore opens, and sodium ions flow down the electrochemical gradient into the cell. Thereafter, a fast inactivation "lid" formed by the cytoplasmic linker between DIII and DIV occludes the pore (Fig. 1, C–E). The protein returns to its resting conformation on repolarization. Individual voltage sensors have unique roles in these rapid gating events. Using voltage-clamp fluorimetry (VCF) to detect motion of each S4 segment in $Na_V1.4$ channels (Fig. 1, F and G), Bezanilla and colleagues demonstrated that movements of the sensors in DI, DII, and DIII correlate with activation, whereas DIII and DIV are coupled to fast inactivation and recovery (Cha et al., 1999; Chanda and Bezanilla, 2002; Chanda et al., 2004).

Upon prolonged depolarization, Na_V channels progressively enter the slow inactivation (SI) state from which they are also slow to recover. Indicating that several conformation states are involved in SI gating, the kinetics of the development of SI show multiple time constants and the rate of recovery from SI slows with progressively longer depolarizing pulses (Toib et al., 1998; Vilin and Ruben, 2001). This complex response to long-lasting depolarization propagates from the cellular to organ level to mediate important aspects of physiology; thus, SI endows neuronal tissues with memory of previous excitation (Toib et al., 1998), prevents excitation of skeletal muscle by mild hyperkalemia (Bendahhou et al., 2002), and affects the conduction velocity and excitability of cardiac tissue (Shaw and Rudy, 1997).

Studies seeking to identify an SI gate in Na_V channels have implicated sites throughout the channel, including the outer portion of the ion conduction pore, the inner pore region, and the voltage-sensor domains. Using VCF to assess changes in the environment of the four S4 segments in $Na_V1.4$, we find that the magnitude, voltage dependence, and time course for SI development and recovery track slow immobilization and restoration of mobility of the voltage sensors in DI, DII, and DIII. Evidence for direct coupling

Correspondence to Steve A.N. Goldstein: goldstein@brandeis.edu

J.R. Silva's present address is Dept. of Biomedical Engineering, Washington University, St. Louis, MO 63130.

Abbreviations used in this paper: K_V, voltage-gated potassium; Na_V, voltage-gated sodium; SI, slow inactivation; TMRM, tetramethylrhodamine maleimide; TTX, tetrodotoxin; VCF, voltage-clamp fluorimetry.

The Rockefeller University Press $30.00
J. Gen. Physiol. Vol. 141 No. 3 309–321
www.jgp.org/cgi/doi/10.1085/jgp.201210909

of DI and DII immobilization and development of SI is provided by suppression of both by tetrodotoxin (TTX). In our companion paper in this issue (Silva and Goldstein), we evaluate $Na_V1.4$ with a mutation that causes hyperkalemic periodic paralysis (L689I) (Bendahhou et al., 2002) and confirm coupling of voltage-sensor immobilization and SI, demonstrating correlated perturbations of sensor movements and changes in SI, corroborating the role of DIII in both onset and recovery, and offering a model that recapitulates the voltage dependence and kinetics of SI based on VCF-determined movements of the voltage sensors in DI, DII, and DIII in wild-type and L689I $Na_V1.4$ channels.

MATERIALS AND METHODS

Cut-open oocyte recording

The cRNA for the β subunit (NCBI Protein database accession no. AAH94523.1) of the rat skeletal muscle sodium channel and α-subunit $Na_V1.4$ (NCBI Protein database accession no. CAA76659.1) was produced in pBSTA and injected at a 1:2 molar ratio (40 ng per cell total) into *Xenopus laevis* oocytes as reported

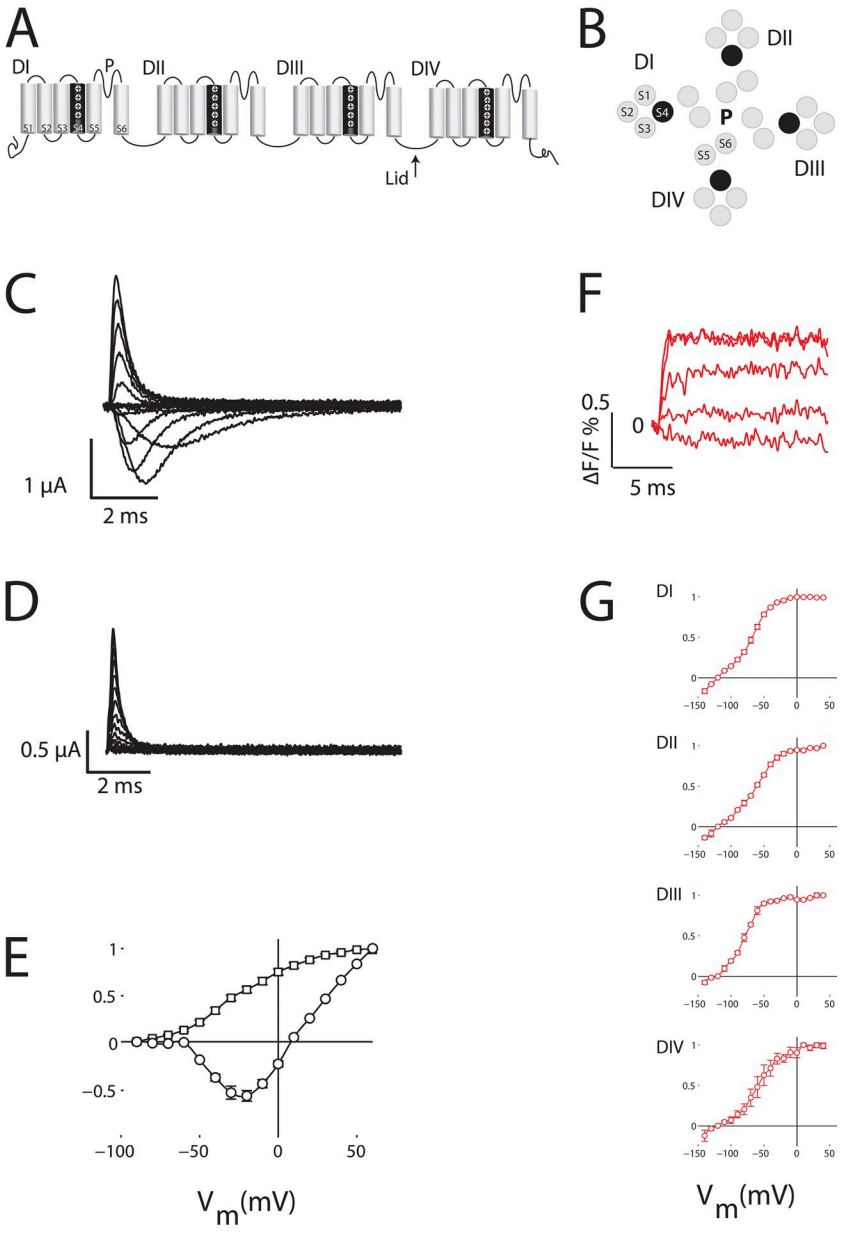

Figure 1. $Na_V1.4$ channel ionic current, gating current, and site-specific fluorescent signals. $Na_V1.4$ currents (black traces) were measured using cut-open oocyte clamp to achieve fast temporal resolution (Stefani et al., 1994) as described in Materials and methods. Changes in fluorescence magnitude ($\Delta F/F_0$; red traces) studied in four channels (DI-S216C, DII-S660C, DIII-L115C, and DIV-S1436C) after conjugation to TMRM. Groups of three to six cells reported as mean ± SEM in E and G. (A) Drawing of the $Na_V1.4$ pore-forming subunit indicating four domains, each with six transmembrane segments; each S1–S4 group forms a voltage sensor, and the four S5–S6 spans are reentrant pore loops that create a single conduction pore. The S4 spans (light gray) are indicated (+) to have multiple arg and lys residues that carry the majority of the gating charge. "Lid" indicates hydrophobic triplet on the DIII–DIV linker that is responsible for fast inactivation. (B) Drawing represents the spatial arrangement of four voltage sensors around a central ion conduction pore. (C) Sodium currents. Activation and fast inactivation of ionic current are apparent with steps from a holding voltage of −100 mV to test potentials of −90 to +60 mV for 60 ms (10 ms shown) in 10-mV steps with a 10-s interpulse interval. For all recordings of ionic currents, gating currents were subtracted. (D) Gating current recorded as in C, with 2 µM TTX in the bath to block ionic current. (E) Channel current/voltage (I/V; circles) and gating current/voltage (Q/V; squares) relationships. Protocol as in C and D. Conductance was calculated by normalizing the current to the driving force (E_{rev} = 7.9 mV), which was fit with a Boltzmann of the form

$$1 / \left(1 + e^{\frac{zF}{RT}(V - V_{mid})} \right),$$

giving a half-maximal voltage (V_{mid}) of −29.1 mV and z = 2.4. For the Q/V relationship, the fit gave V_{mid} = −27.5 mV and z = 1.1. (F) VCF measurements. Fast changes in fluorescence compared with baseline ($\Delta F/F_0$) for DI-S216C channels studied by applying steps from a holding potential of −120 mV to test potentials of −140 to 40 mV in 10-mV steps; traces at −140, −100, −60, −20, and 20 mV are shown. (G) Fluorescence/voltage (F/V) relationships for each of the four Nav1.4 domains. Fits as in E gave DI: V_{mid} = −74.6 mV and z = 1.3; DII: V_{mid} = −69.4 mV and z = 1.1; DIII: V_{mid} = −82.4 mV and z = 1.7; and DIV: V_{mid} = −70.6 mV and z = 1.5.

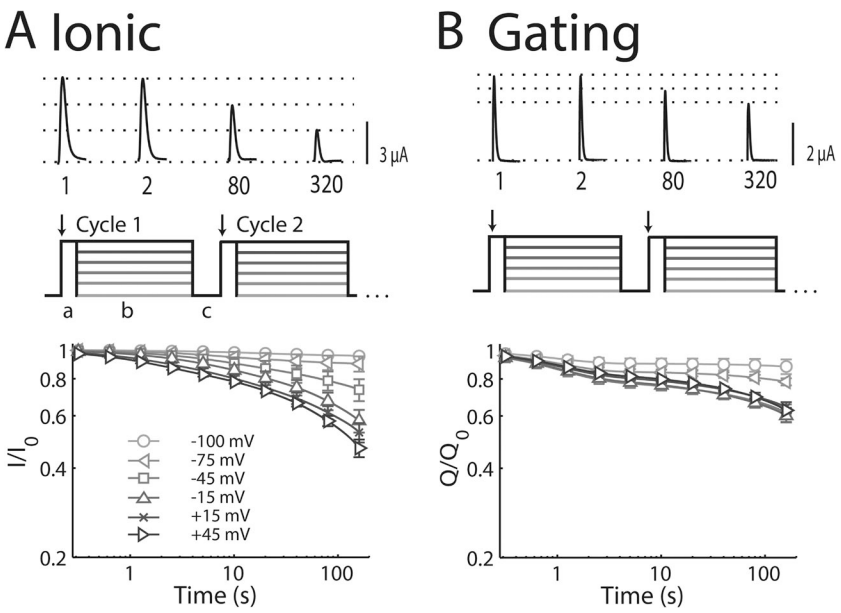

Figure 2. SI onset: Ionic and gating currents. Groups of 4–14 cells reported as mean ± SEM. (A) SI is probed by 320 repetitions of a triple-pulse protocol from a holding potential of −100 mV. A 5-ms test pulse to +45 mV was used to measure peak current (phase a); SI was induced by a 500-ms pulse at −100, −75, −45, −15, 15, or 45 mV (phase b); and a 30-ms pulse at −100 mV was used (phase c) to allow for recovery from fast inactivation before the next test pulse. Above protocol, sample traces from cycles 1, 2, 80, and 320 show progressive decrease in peak current with SI at +45 mV. Parameters for SI onset are reported in Table 1. (B) Loss of gating current with SI induced as in A. (Top) Sample traces from cycles 1, 2, 80, and 320 show progressive reduction in peak gating current with SI at +45 mV. (Bottom) Plot of the gating charge (Q, the integral of the gating current) with time at different potentials.

previously (Chanda and Bezanilla 2002). Oocytes were incubated at 16.5°C for 2–5 d in solution with (mM) 96 NaCl, 4 KCl, 1.8 $CaCl_2$, 1 $MgCl_2$, 5 HEPES, and 0.1 EDTA, and 1% penicillin-streptomycin, pH 7.4. Recordings were performed using an amplifier (CA-1B; Dagan Corporation) coupled to an A/D converter (Digidata 1320; Molecular Devices) with Clampex and Clampfit software (v10; Molecular Devices) for acquisition and analysis. Temperature was maintained at 19°C with a controller (HCC-100A; Dagan Corporation). The internal solution was (mM): 113 NMG-Mes, 2 Na-Mes, 20 HEPES, and 2 EGTA, pH 7.4. The external solution was composed of (mM): 95 NMG-Mes, 20 Na-Mes, 20 HEPES, and 2 $Ca\text{-}Mes_2$, pH 7.4. Capacitance and leak were subtracted manually. In ionic current studies, gating current was recorded with 2 µM TTX in the external solution and subtracted.

Fluorescence measurements

Oocytes were labeled with 10 µM tetramethylrhodamine maleimide (TMRM; Invitrogen) in a depolarizing solution (mM: 110 KCl, 1.5 $MgCl_2$, 0.8 $CaCl_2$, and 10 HEPES, pH 7.4) on ice for 20 min. TMRM stock solution was 10 mM in DMSO and stored at −80°C. A tungsten halogen lamp with a 250-W filament powered by a 24-V linear power supply served as the light source. The lamp output was interrupted with a TTL-triggered shutter (Sutter Instrument) to minimize photobleaching of the probe. After collimation (Thorlabs Inc.), light was carried to the microscope via a liquid light guide (Sutter Instrument) and coupled to the microscope via a collimating adapter (EXFO). A 40× water-immersion objective with a numerical aperture of 1.0 and working distance of 2.1 mm (Plan Acrochromat; Zeiss) was used. Light measurements were made with a photodiode (PIN-040A; United Detector Technology) mounted on an XY axis manipulator (Thorlabs Inc.) at the microscope epifluorescence port. The photodiode was attached to the integrating headstage of a patch-clamp amplifier (Axopatch-200A; Molecular Devices) for low noise amplification of the photocurrent. A circuit with a 22.5-V battery and 6-GΩ resistance was used to remove integration spikes by offsetting current into the summing junction of the headstage. The fluorescence emission was focused onto the photodiode active area using an achromatic doublet (Thorlabs Inc.) with a focal distance of 25 mm.

Data analysis

Parameters were determined by fits of the raw data: SI onset (Table 1) and SI recovery (Table 2). For each trace, three exponentials were fit to the raw data using the "lsqcurvefit" function in MATLAB (MathWorks), which implements a trust-region reflective optimization algorithm. Each of the three exponentials was

TABLE 1

Fractional magnitudes of time constants for ionic current, gating current, and fluorescence during the onset of SI

Channel variant (measured parameter)	A_F	A_I	A_S	C	*n*
WT (I)	0.13 ± 0.01	0.11 ± 0.01	0.51 ± 0.06	0.25 ± 0.05	14
WT (Q) (2 µM TTX)	0.13 ± 0.01	0.03 ± 0.01	0.35 ± 0.03	0.49 ± 0.03	4
DI (F)	0.25 ± 0.02	0.17 ± 0.03	0.28 ± 0.03	0.30 ± 0.04	6
DII (F)	0.23 ± 0.06	0.27 ± 0.04	0.27 ± 0.02	0.23 ± 0.06	6
DIII (F)	0.28 ± 0.05	0.17 ± 0.05	0.26 ± 0.06	0.30 ± 0.05	8
DIV (F)	0.29 ± 0.03	0.08 ± 0.04	0.16 ± 0.03	0.46 ± 0.03	6

First, SI of ionic current at +45 mV was fit using three exponentials with time constants for fast, intermediate, and slow components: τ_F = 1.8 ± 0.2 s, τ_I = 13.1 ± 1.1 s, and τ_S = 195 ± 33 s. Because the three time constants span the time domains of our protocol, they can be held constant and used to describe data from ionic, gating, and fluorescence measurements by varying the fractional magnitude of each component (Fig. S1). The table shows the fractional magnitude of each component for all studies in this article. *n*, the number of cells studied; WT, wild-type channel; DI, DII, DIII, and DIV indicate channels with the single site changes DI-S216C, DII-S660C, DIII-L115C, and DIV-S1436C, respectively; I, current assessed after subtraction of Q; F indicates a fit to fluorescence.

allowed to range in a unique time scale: from 1 to 10 s, 10 to 100, and 100 to 1,000 s. Points logarithmically distributed in time were then plotted according to the fit. Later to compare traces quantitatively, it was useful to reduce the number of parameters and set the time constants to be invariant, while only the magnitudes were allowed to vary.

Online supplemental material

Fig. S1 is provided to demonstrate the success of fitting SI traces by varying the magnitudes of three exponentials, while leaving the time constant for each unchanged. It is available at http://www.jgp.org/cgi/content/full/jgp.201210909/DC1.

RESULTS

Sodium current: Onset of SI

SI develops with repetitive or prolonged activity, limiting the availability of channels that open on depolarization so that peak currents become progressively smaller. In this work, SI is induced using a triple-pulse protocol repeated 320 times (Fig. 2 A); each cycle includes a 5-ms step to +45 mV to measure peak current (phase a), an SI induction phase of 500 ms at various voltages (phase b),

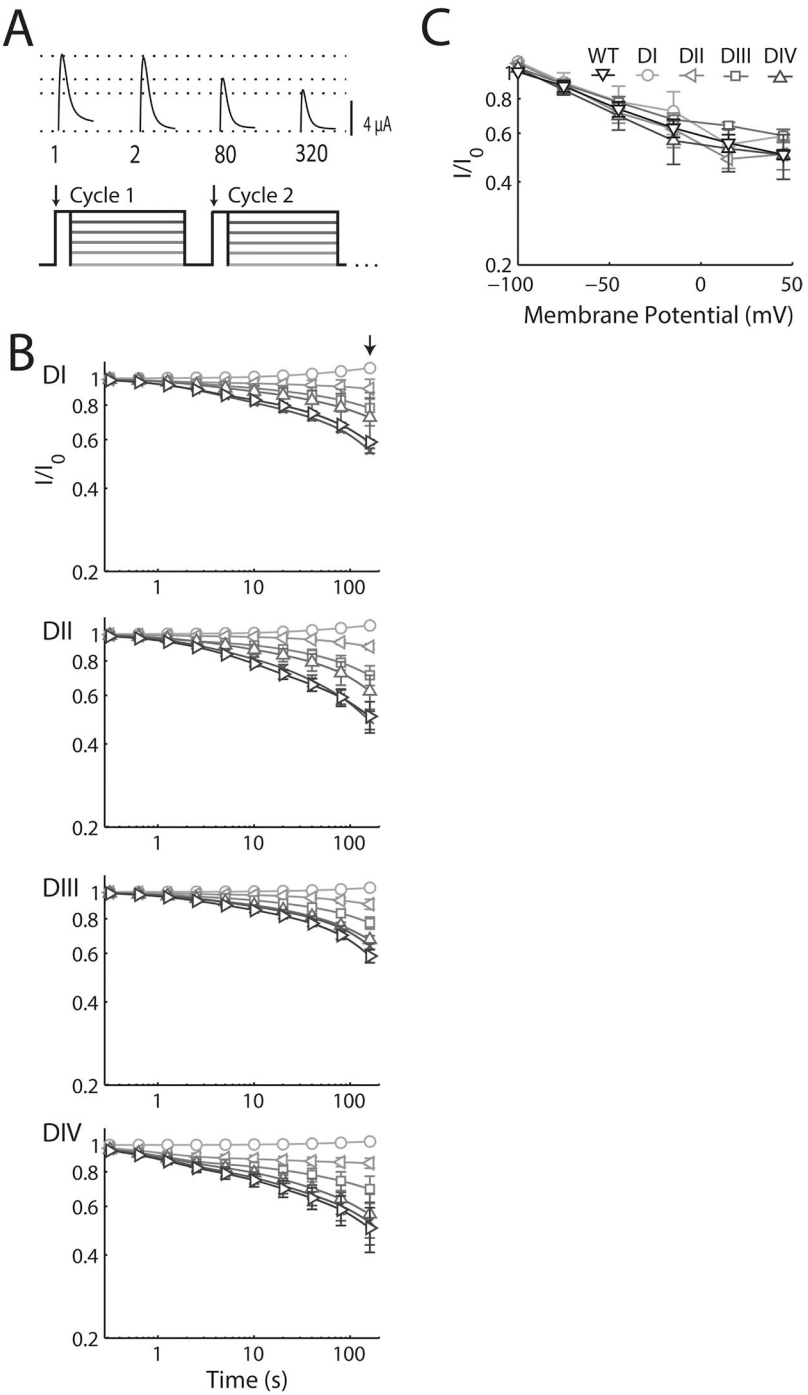

Figure 3. Single cysteine substitutions do not alter SI. Ionic currents for WT, DI-S216C, DII-S660C, DIII-L115C, or DIV-S1436C channels measured using the protocol in Fig. 2 A. Gating current is not subtracted from ionic current. Data for groups of four to six cells are shown as mean ± SEM. (A) Representative traces for the DI-S216C channel resulting from repetitive pulse to induce SI. (B) Voltage and time dependence of SI in the four mutant channels remain largely unchanged with the introduction of the cysteine and conjugation of the fluorophore (see C). (C) When a fluorophore is conjugated to each of four cysteine mutants, a slight shift to higher potentials in DI and DIII is observed compared with WT SI at 160 s. At +45 mV, this shift is seen as a trend for DI ($P = 0.15$) and significant for DIII ($P < 0.05$).

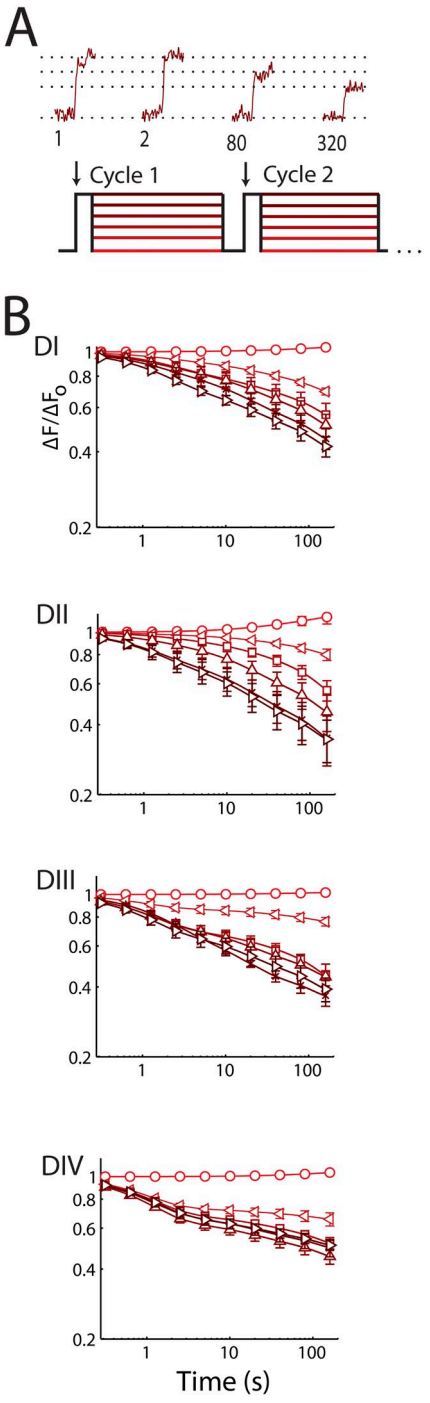

Figure 4. Voltage-sensor immobilization is observed with SI in all four domains. Changes in fluorescence magnitude ($\Delta F/F_0$) of TMRM conjugated to each domain via DI-S216C, DII-S660C, DIII-L115C, or DIV-S1436C. The mean ± SEM for groups of six to eight cells is reported. (A) Fluorescence. (Top) Application of the triple-pulse protocol reveals reduction in the $\Delta F/F_0$ with increasing cycle number: 4 ms before and 4 ms after the test step to +45 mV (phase a) for the indicated pulse is shown. (B) Time-dependent change in the magnitude of $\Delta F/F_0$ for the four channels on log–log plots using the triple-pulse protocol described in Fig. 2 A. Parameters are shown in Table 1. DI and DII show changes with voltage and cycle number that are most reminiscent of SI.

and a third phase (c) at the holding voltage of −100 mV lasting 30 ms, a duration sufficient to allow recovery from fast inactivation, but not SI, before the next pulse.

SI depends on induction potential and cycle number; with greater depolarization, a larger fraction of the channels moves into SI states (Fig. 2 A). After 320 cycles to an induction potential of +45 mV, peak currents are decreased by 53 ± 3%. The decrease in current extends over a wide range of timescales (1, 10, and 100 s), requiring description in terms of multiple time constants. SI onset during 320 cycles (∼160 s) can be approximated by three exponential time constants (Fig. S1), τ_{Fast} = 1.8 ± 0.2 s, $\tau_{Intermediate}$ = 13.1 ± 1.1 s, and τ_{Slow} = 195 ± 33 s, which have fractional magnitudes of 0.13 ± 0.01, 0.11 ± 0.01, and 0.51 ± 0.06, respectively, and a constant remainder (C) of 0.25 ± 0.05 (Table 1). τ_{Slow} and C reflect SI continuing in time scales beyond those well studied with 320 cycles and must, therefore, be considered with caution as suggestive; these transitions with τ > 100 s are often referred to as ultraslow (Sandtner et al., 2004; Szendroedi et al., 2007).

Gating current: Onset of SI

Na_V gating currents are generated by charges in the channel protein that move with changes in transmembrane potential and are primarily caused by arg and lys residues in the four S4 segments. Gating currents are recorded here by application of the pore blocker TTX at 2 µM to suppress all sodium ion permeation through the pore (Fig. 1 D). When the triple-pulse protocol is applied, the charge carried by the gating currents decreases with increasing potential and cycle number (Fig. 2 B). The magnitude, voltage dependence, and kinetics of gating charge suppression are observed to be quite different than for SI (Fig. 2 A). After 320 cycles to +45 mV, peak gating charge decreases by just 36 ± 1% and, of particular note, the log–log plot is flat in the 10-s time scale (Fig. 2 B), consistent with ∼70% reduction in the fractional magnitude of $\tau_{intermediate}$ (Table 1).

Movement of S4 segments by VCF: Onset of SI

To examine movement of individual voltage sensors, rather than their aggregate manifestation in the gating current, we applied VCF to the same four $Na_V1.4$ channels created by Bezanilla and colleagues to study fast gating events, DI-S216C, DII-S660C, DIII-L115C, and DIV-S1436C (provided by F. Bezanilla, University of Chicago, Chicago, IL; Cha et al., 1999; Chanda and Bezanilla, 2002; Chanda et al., 2004). Each channel bears a cys in place of a natural S4 span residue to permit modification by a fluorophore to monitor sensor movement. Bezanilla and colleagues studied these four mutant channels because they do not disrupt rapid gating. Similarly, we find that the mutations allow for the study of SI (Fig. 3).

Whereas activation of DI-S216C channels produces rapid voltage-dependent changes in fluorescence to a stable level (Fig. 1 F), repetitive activation cycles to induce SI decrease peak fluorescence (Fig. 4 A), indicating that the DI sensor slowly becomes immobile. Unexpectedly, the magnitude, voltage dependence, and kinetics of DI sensor immobilization (Fig. 4 B) resemble SI of ionic currents (Fig. 2 A) rather than gating currents (Fig. 2 B). Thus, SI and DI slow immobilization show voltage-dependent changes from −100 to +15 mV across the three time domains studied. Similarly, VCF with DII-S660C channels reveals slow immobilization of the DII sensor resembling SI of ionic currents rather than gating currents (Fig. 4 B). In contrast, immobilization of DIII bears some likeness to SI but develops at more hyperpolarized potentials (seen as clustering of

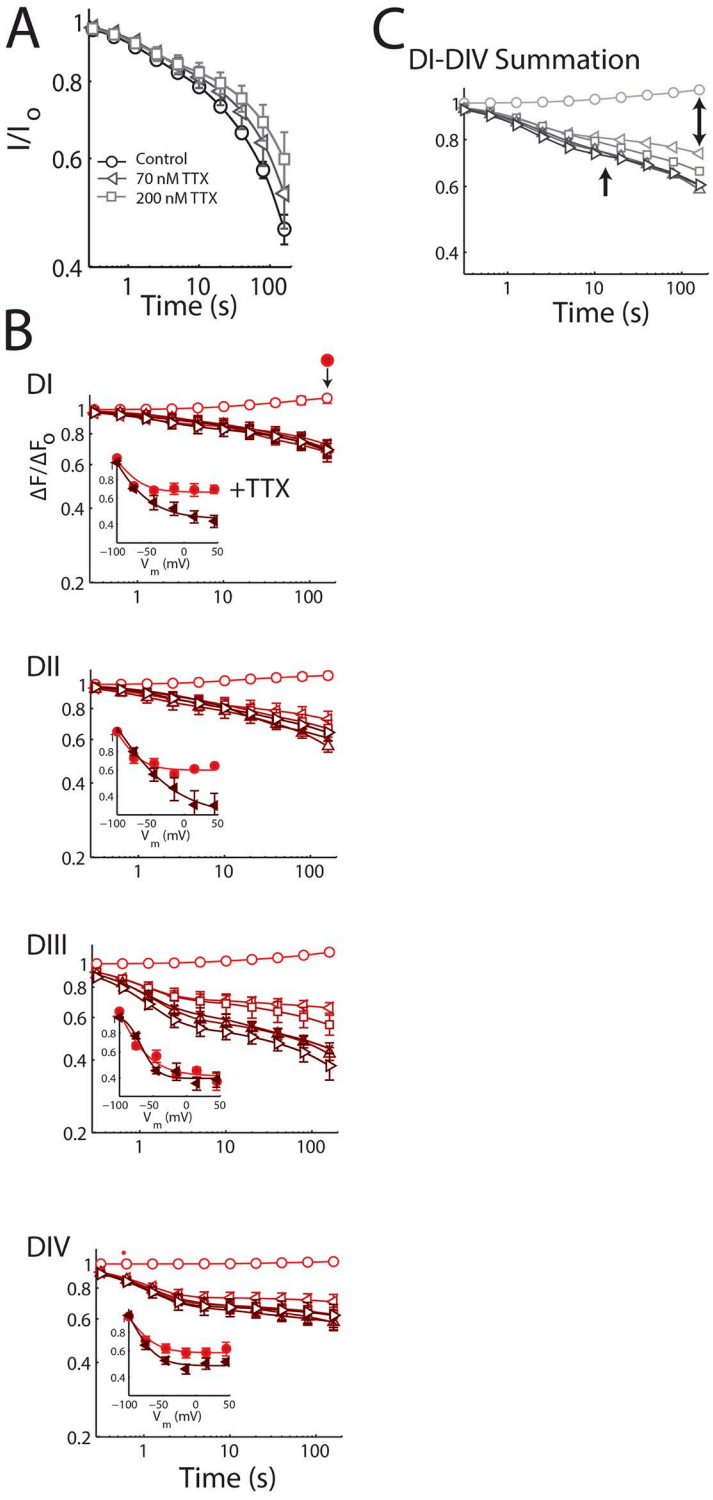

Figure 5. Immobilization of DI and DII voltage sensors is suppressed by TTX. Changes in the fluorescence magnitude ($\Delta F/F_0$) of TMRM conjugated to each domain via DI-S216C, DII-S660C, DIII-L115C, or DIV-S1436C in the presence of 2 µM TTX. The mean ± SEM for groups of 5–14 cells is reported. (A) Ionic currents. SI in wild-type channels in the absence and presence of the indicated levels of TTX by the protocol shown in Fig. 2 A. TTX inhibition decreases SI (P = 0.038 for 200 nM vs. control). (B) Fluorescence recordings as in Fig. 4 B with TTX. Parameters are shown in Table 2. DI and DII voltage sensors are significantly affected and are now reminiscent of gating currents. Insets compare immobilization for the indicated domain at 160 s with TTX (bright circles) and without TTX (dark triangles). (C) Expected gating charge immobilization based on fluorescence measurements. Each domain was assumed to carry 25% of the gating charge, and the traces represent the sum (see Results).

TABLE 2

Fractional magnitudes of time constants for ionic current, and fluorescence during the onset of SI in the presence of TTX

Channel variant (measured parameter)	A_F	A_I	A_S	C	*n*
WT (I) 70 nM TTX	0.12 ± 0.02	0.07 ± 0.03	0.50 ± 0.07	0.31 ± 0.09	7
WT (I) 200 nM TTX	0.12 ± 0.03	0.06 ± 0.02[a]	0.42 ± 0.10	0.40 ± 0.10	11
DI (F) + 200 nM TTX	0.13 ± 0.06	0.05 ± 0.02[a]	0.24 ± 0.07	0.59 ± 0.06[a]	6
DII (F) + 200 nM TTX	0.13 ± 0.04	0.11 ± 0.04[a]	0.22 ± 0.05	0.54 ± 0.03[a]	6
DIII (F) + 200 nM TTX	0.39 ± 0.05	0.05 ± 0.03	0.27 ± 0.07	0.30 ± 0.08	6
DIV (F) + 200 nM TTX	0.27 ± 0.05	0.01 ± 0.00	0.09 ± 0.03	0.63 ± 0.08	5

τ_F, τ_I, and τ_S and channel variant abbreviations are as in Table 1. p-values were calculated to evaluate differences between WT signals and those with TTX.
[a]Significant differences, $P < 0.05$.

the traces at potentials more positive than −45 mV). DIV immobilization is also more rapid to develop than SI and most closely resembles gating currents in small fractional amplitudes of $\tau_{intermediate}$ (Table 1).

TTX inhibits SI onset and movement of sensors in DI and DII

The observed difference between gating and ion currents during SI is found to be caused in large part by the 2 µM TTX present in the bath during gating studies. Thus, the application of the pore blocker at low levels that inhibit only a portion of the ionic current is observed to suppress SI and, as TTX concentration increases, SI decreases (Fig. 5 A). Suppression of SI is significant in the intermediate time domain with the addition of just 0.2 µM TTX (Table 2). When VCF is performed with 2 µM TTX (the level added to study gating currents), significant suppression of slow immobilization of the DI and DII sensors in the intermediate time domain is observed (Fig. 5 B and Table 2). Potent suppression is apparent for DI and DII as well in the parameter C that reflects the summation of immobilization over the entire protocol (Fig. 5 B, insets, and Table 2). Although TTX-induced changes in SI of the DIII and DIV sensors did not reach significance, a trend was observed in the magnitude of $\tau_{Intermediate}$ for both domains and τ_{Slow} for DIV ($P < 0.1$) (Table 2). The impact of TTX on SI is perhaps not a surprise given that it shows use-dependent block (Lönnendonker, 1989) and indicates that gating current assessment can be confounded by the blocker, a concern supported by others (Capes et al., 2012).

Given that fluorescence changes are dependent on the movement of S4 sensors, we expect the summation of the traces in the presence of TTX to reflect gating charge immobilization, although correlation between gating currents and fluorescence will be imperfect because they report on different processes (Mannuzzu et al., 1996; Chanda and Bezanilla, 2002). To make the comparison, we estimate that each sensor carries 25% of gating charge (Sheets et al., 2000; Sokolov et al., 2008). A summation of the traces from Fig. 5 B in Fig. 5 C does resemble gating charge immobilization, particularly in the flattening of the curves in the 10-s region of the plot. In contrast, VCF shows inactivation at −75 mV (Fig. 5 C, double arrow) that is not observed in the

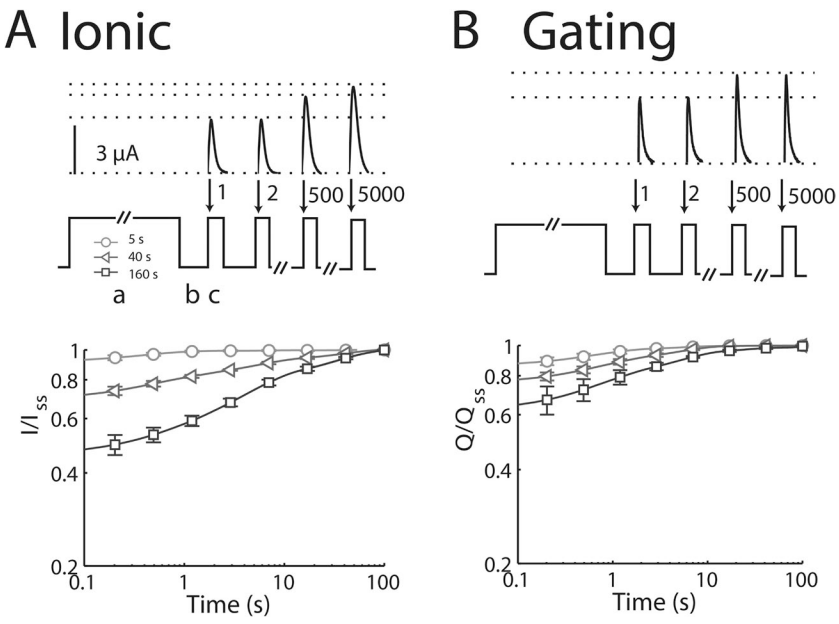

Figure 6. Recovery from SI: Ionic and gating currents. Changes in ionic and gating current as channels recover from SI. The mean ± SEM for groups of four to five cells is reported. (A) Sodium current. (Top) Recovery from SI is probed after induction pulses to +45 mV for 5, 40, or 160 s (phase a) during 5,000 cycles of 20 ms at −100 mV (phase b), followed by 4 ms at +45 mV when peak current is recorded (phase c). Sample traces from cycles 1, 2, 500, and 5,000 show the recovery of peak current. (Bottom) Voltage and cycle dependence of recovery from SI on log–log plots of peak current normalized to the steady-state (change of <1%) current after recovery. Parameters for recovery from SI are shown in Table 3. (B) Gating current. Recovery from SI is probed as in A, with 2 µM TTX.

TABLE 3

Recovery fractional magnitudes of recovery from SI

Channel variant (measured parameter)	Pulse	A_F	A_I	A_S	C	*n*
	s					
WT (I)	5	0.10 ± 0.02 (0.89)	0.00 ± 0.00 (0.05)	0.01 ± 0.01 (0.06)	0.89 ± 0.03	4
WT (I)	40	0.13 ± 0.02 (0.32)[a]	0.15 ± 0.04 (0.37)[a]	0.12 ± 0.01 (0.31)[a]	0.60 ± 0.03	4
WT (I)	160	0.07 ± 0.03 (0.10)[a,b]	0.35 ± 0.02 (0.50)[a]	0.28 ± 0.02 (0.41)[a]	0.30 ± 0.05	4
WT (Q)	5	0.10 ± 0.02 (0.73)	0.03 ± 0.02 (0.25)	0.00 ± 0.00 (0.02)	0.86 ± 0.03	5
WT (Q)	40	0.12 ± 0.02 (0.48)[a]	0.12 ± 0.02 (0.51)[a]	0.03 ± 0.03 (0.01)	0.76 ± 0.03	5
WT (Q)	160	0.15 ± 0.03 (0.39)[a]	0.18 ± 0.07 (0.48)[a]	0.05 ± 0.01 (0.13)[b]	0.62 ± 0.08	5
DI (F)	5	0.17 ± 0.04 (0.98)	0.00 ± 0.00 (0.02)	0.00 ± 0.00 (0.00)	0.83 ± 0.04	7
DI (F)	40	0.22 ± 0.05 (0.53)[a]	0.19 ± 0.04 (0.46)[a]	0.00 ± 0.00 (0.01)	0.59 ± 0.04	7
DI (F)	160	0.13 ± 0.03 (0.35)[a]	0.18 ± 0.03 (0.46)[a]	0.08 ± 0.03 (0.20)[a,b]	0.61 ± 0.04	7
DII (F)	5	0.20 ± 0.08 (0.94)	0.01 ± 0.01 (0.06)	0.00 ± 0.00 (0.00)	0.79 ± 0.07	3
DII (F)	40	0.12 ± 0.10 (0.36)	0.21 ± 0.02 (0.61)	0.01 ± 0.01 (0.03)	0.66 ± 0.09	3
DII (F)	160	0.13 ± 0.11 (0.28)	0.22 ± 0.07 (0.49)	0.11 ± 0.03 (0.23)[a,b]	0.54 ± 0.06	3
DIII (F)	5	0.34 ± 0.08 (0.89)	0.04 ± 0.02 (0.09)	0.01 ± 0.01 (0.02)	0.61 ± 0.06	6
DIII (F)	40	0.16 ± 0.08 (0.32)[a]	0.18 ± 0.05 (0.36)	0.17 ± 0.03 (0.32)[a]	0.48 ± 0.06	6
DIII (F)	160	0.04 ± 0.04 (0.07)[a]	0.23 ± 0.01 (0.38)[a]	0.32 ± 0.03 (0.55)[a,b]	0.41 ± 0.02	6
DIV (F)	5	0.08 ± 0.05 (0.72)	0.03 ± 0.01 (0.28)	0.00 ± 0.00 (0.00)	0.89 ± 0.05	7
DIV (F)	40	0.03 ± 0.02 (0.12)[a]	0.14 ± 0.02 (0.59)	0.07 ± 0.03 (0.29)[a]	0.76 ± 0.04	7
DIV (F)	160	0.07 ± 0.03 (0.19)[a]	0.11 ± 0.02 (0.31)[b]	0.18 ± 0.03 (0.50)[a,b]	0.65 ± 0.05	7

Similar to SI onset, recovery from SI can be fit with three time constants, $\tau_F = 0.6 \pm 0.3$ s, $\tau_I = 4.5 \pm 1.1$ s, and $\tau_S = 43.1 \pm 4.8$ s, which were found by fitting the recovery of the wild-type ionic current after a 160-s depolarizing pulse to +45. The fractional magnitudes below are for pulses to +45 mV lasting 5, 40, and 160 s. The absolute values correlate to the fraction inactivated during onset, which are described in Tables 1 and 2. To compute significance differences in time constants between durations, magnitudes were normalized to the fraction inactivated (shown in parentheses). For example, after the 5-s pulse, the fraction of current inactivated with τ_F was 0.91. p-values were computed to compare fraction inactivated with a given τ. I, the ionic current recovery in Fig. 6 A; Q, the gating current recovery in Fig. 6 B; DI, DII, DIII, and DIV, the fluorescence recoveries in Fig. 7 B. Channel variant abbreviations as in Table 1.

[a]Significantly different ($P < 0.05$) from the 5-s pulse.

[b]Significantly different from 40 s (160 pulses).

gating charge perhaps because of movement of adjacent transmembrane segments that register differently in the two measures. Assigning up to 35% of the charge to any sensor at the expense of the others does not significantly affect the plot (not depicted).

Recovery from SI

Channel availability is a balance between development of SI and recovery from SI. To study recovery, SI is induced by pulses to +45 mV that last 5, 40, or 160 s followed by two steps that are repeated 5,000 times: the first step allows for recovery for 20 ms at the holding voltage of −100 mV, and the second step measures recovery of peak current at +45 mV (Fig. 6 A). As reported by others (Hayward et al., 1997; Toib et al., 1998; Melamed-Frank and Marom, 1999), we observe recovery time constants to increase with longer induction pulses. In the time range studied here, recovery is adequately fit by three time constants ($\tau_{Fast} = 0.6 \pm 0.3$ s, $\tau_{Intermediate} = 4.5 \pm 1.1$ s, and $\tau_{Slow} = 43.1 \pm 4.8$ s), with fractional magnitudes that shift to longer time scales with longer induction (Table 3). Thus, all recovery of ionic current occurs with τ_{Fast} after inductions lasting 5 s. With 40-s inductions, recovery is spread equally across

TABLE 4

Boltzmann fits to F-V curves

Channel variant	A_1	B_1	C_1	A_2	B_2	C_2	D
DI	0.73	0.0067	12.13	1.44	0.005	31.8	−1.1
DII	0.43	0.0087	10.99	0.98	0.052	36.3	−0.4
DIII	0.43	0.0001	8.16	0.70	0.010	20.7	−0.1
DIV	0.81	0.0062	12.76	1.57	0.008	41.47	−1.4

For F-V curves, two Boltzmann functions fit the curve well: $\sum_{i=1}^{2} \frac{A_i}{1 + B_i e^{-V_m/C_i}} + D$. In each case, only one Boltzmann described voltage dependence above −100 mV. To derive the steady-state activated probability for modeling purposes, A_1 was set to 1 and D to 0. The values predicted by this normalized function, which used B_1 and C_1, were used to calculate the steady-state occupancy. Channel variant abbreviations as in Table 1.

the three time constants, and with 160-s inductions, 90% of recovery occurs with $\tau_{Intermediate}$ and τ_{Slow}. Recovery time constants for gating currents vary less with induction time (Fig. 6 B and Table 3).

Like recovery of ionic currents, VCF shows that restoration of voltage-sensor mobility in all four domains shifts to longer time scales with longer inductions; that is, the amplitude of τ_S is greater after 160 s rather than after 40- or 5-s pulses (Fig. 7 and Table 3). This hallmark of recovery from SI is most prominent in DIII. Thus, 90% of DIII sensor recovery occurs with τ_{Fast} after a 5-s induction. After a 40-s induction, recovery is spread evenly across the three time scales. With 160-s inductions, 93% of recovery occurs with $\tau_{Intermediate}$ and τ_{Slow}. In contrast, the sensors in DI, DII, and DIV recover more rapidly than DIII and show less induction time–dependent shift to $\tau_{Intermediate}$ and τ_{Slow}. Of note, the change in fluorescence with SI induced by steps to +45 mV (Fig. 4) is restored by recovery at −100 mV (Fig. 7), and this demonstrates that a potential confounding variable in these studies, bleaching of the reporter fluorophore (TMRM), did not prove to be a problem.

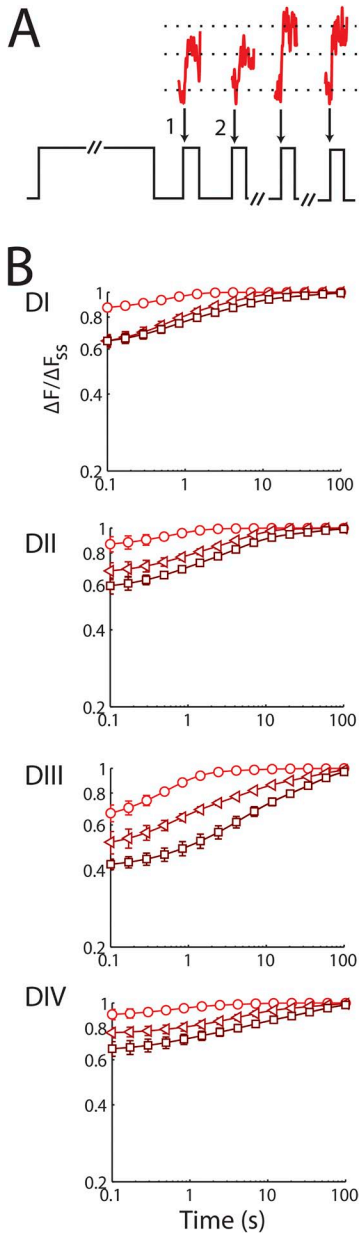

Figure 7. Recovery from SI is reflected in restored voltage-sensor mobility, especially DIII. Changes in fluorescence magnitude ($\Delta F/F_0$) studied as channels recover from SI. The mean ± SEM for groups of four to eight cells is reported. (A) Changes in $\Delta F/F_0$ with DI-S216C by the protocol shown in Fig. 6 A, with duration of 40 ms in phase b. (B) Voltage and cycle dependence of recovery from SI of $\Delta F/F_0$ for the four channels on log–log plots. Parameters are listed in Table 3; changes in DIII are notable.

Modeling voltage-sensor inactivation

To formalize correlations of voltage-sensor movements and SI quantitatively, we parameterized discrete-state Markov models to fit VCF recordings (Fig. 8). A model adequate to recapitulate SI across observed voltages and time scales has five sequential states: one closed, one active, and three inactive (C↔A↔I1↔I2↔I3). Accordingly, the fluorescence signal in the experiments correlates with the C to A transition in the model. As sensors move into the inactive states, the activating transition becomes unavailable and the magnitude of the fluorescence signal decreases. The presence of three inactivating transitions is expected given the success of fitting the experimental data with three independent exponentials (Tables 1 and 2).

The first model transition (C↔A) is orders of magnitude faster (<1 ms) than the rest of the transitions that occur over seconds and is assumed to be in equilibrium so that the steady-state probability that a sensor is in the activated conformation can be used for calculations; steady-state values are derived by fitting F-V curves (Fig. 1) with two saturating Boltzmann functions. In each case, only one Boltzmann function accounted for voltage dependence of a sensor greater than −100 mV, and the second reflected movement at hyperpolarized potentials (Table 4). Rate constants for inactivating transitions are independent of voltage with the exception of recovery for DI and DII, suggesting that voltage acts primarily on the closed to active transition (Table 5).

DISCUSSION

This work shows that the voltage sensors in all four Na_V channel domains slowly immobilize with the development of SI. All four sensors are also restored to mobility with recovery from SI. The sensors do not, however, track these transitions equally well over the times studied (1–160 s). Immobilization of the voltage sensors tracks the onset of SI with a rank order of DI, DII > DIII >> DIV. Consistent with a causal link, TTX significantly

reduces both SI in the intermediate (10-s) time domain and slow immobilization of the sensors in DI and DII. Recovery from SI takes longer when induction pulses are extended, and remobilization of voltage sensors tracks this prolonged recovery time course. DIII is notable for resisting remobilization compared with the other sensors and manifests a time course that correlates with recovery, suggesting that it has a role in the transition to restored mobility. A model is where sensors are trapped in an inactive state after activation recapitulates SI and suggests that the voltage dependence of slow sensor immobilization arises from the closed to active transition.

Our findings show that sensor immobilization with SI is different than gating charge immobilization that develops much more rapidly with fast inactivation. In the latter state, Na_V sensor immobilization follows occlusion of the inner pore by residues on the DIII–DIV linker, and mobility is restored by repolarization in <20 ms. This does not preclude direct transition between the two immobilized states; indeed, mutations in the inner pore can modify the onset of both (McNulty et al., 2006). However, mutating the "lid" to eliminate fast inactivation allows SI to develop more quickly and completely (Featherstone et al., 1996), and this suggests that SI does not require prior entry in the fast inactive state. Although the inner portion of the Na_V channel pore has been implicated in SI by mutations that cause hyperkalemic periodic paralysis (Cummins et al., 1993; Hayward et al., 1999; Bendahhou et al., 2002; Webb and Cannon, 2008), this may be an allosteric effect on sensor movement, as shown here for TTX in the outer pore.

Our demonstration that increasing the concentration of TTX progressively inhibits SI supports the notion that conformational changes in the Na_V channel pore cause SI and are suppressed by the toxin. Studies of mutations (Balser et al., 1996; Vilin et al., 1999; Vilin and Ruben, 2001; Xiong et al., 2003, 2006) and alkali ions that stabilize the open state (Townsend and Horn, 1997) have previously argued for a link between the outer pore and SI. Although Na_V channel SI has been

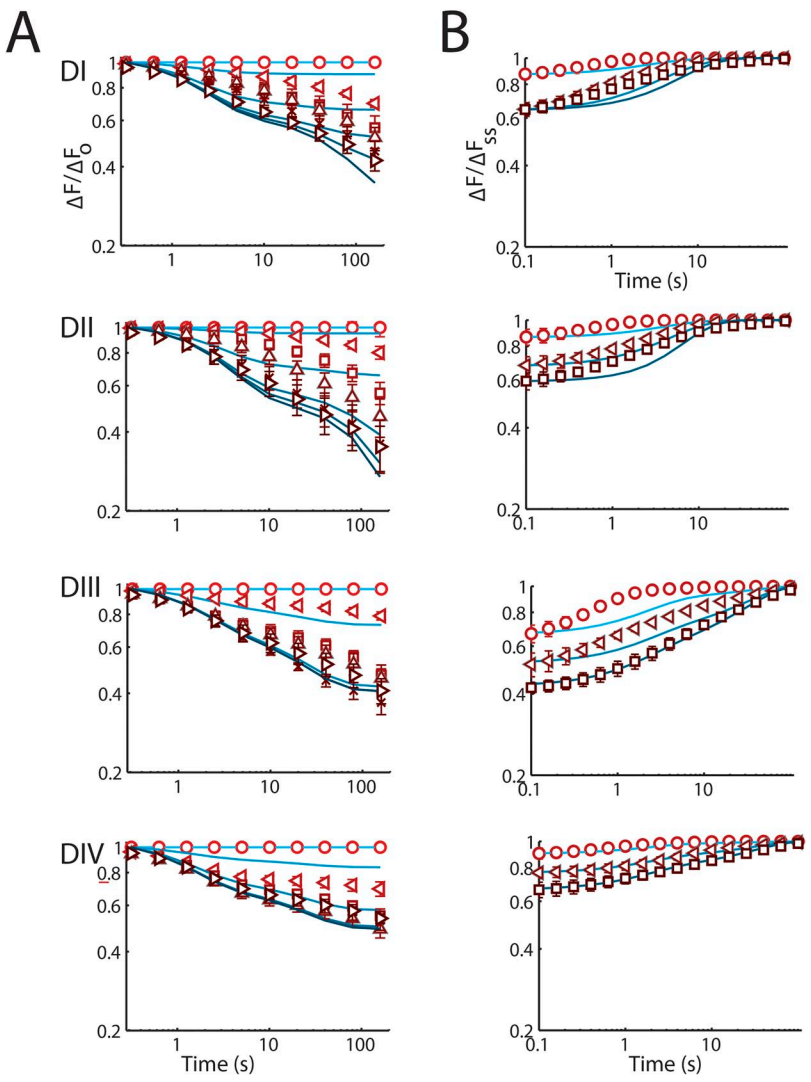

Figure 8. Models of voltage-sensor slow immobilization. Experimental data are shown with symbols, and models are represented by solid blue lines. The effect of the protocol was removed for model fitting by subtracting the minimal changes in voltage-sensor activation observed with pulses to −100 mV. For fitting, experimental recovery is scaled so that it begins recovering from exactly the same fraction where onset terminated. Ionic current recovery is simulated using the same parameters and models used to simulate ionic onset (Table 5). These simplified models are qualitatively similar to the inactivation of the voltage sensors. (A) Model voltage-sensor slow immobilization for all four domains. (B) Model voltage-sensor recovery from slow immobilization for all four domains.

compared with C-type inactivation of voltage-gated potassium (K_V) channels, a process dependent on outer pore collapse, the latter is well described by a single-exponential process and does not change its kinetics of recovery with inducing pulse duration (Toib et al., 1998). These differences may be caused by the coupling of SI and processes in the voltage sensors unique to Na_V channels. For example, voltage sensors in Na_V channels are sensitive to movement of adjacent sensors (Chanda et al., 2004) and, unlike those in K_V channels formed of homotetramers, individual Na_V sensors move over different time scales (Gagnon and Bezanilla, 2010). Thus, it may be different kinetic profiles for individual voltage sensors and their interaction that endow a sensor-linked process like SI with greater kinetic complexity in Na_V channels.

Unlike the sensors in DI, DII, and DIII, we observe immobilization and restored mobility of the DIV sensor to be poorly correlated with the kinetics of both SI development and recovery in the 1–160-s time range. Nonetheless, a role for DIV in SI at times faster than 1 s seems plausible given its demonstrated function in both activation and fast inactivation (Horn et al., 2000). Although 2 µM TTX shows a nonsignificant trend toward impeding slower components of DIV immobilization (Table 2), this may result from a conformational change in DI with SI that is reflected in DIV as a result of strong cooperativity between the two domains (Chanda et al., 2004).

Recent work by others supports our conclusion that there is conformational coupling of the pore and voltage sensors in $Na_V1.4$ (Capes et al., 2012). They find that neutralizing three charges in the S4 span of DIV creates a new pathway that allows omega currents to pass through the sensor domain, and that TTX in the ion conduction pore alters both omega currents and off-gating currents carried by the remaining DIV charges; these effects were not observed in domains I, II, or III. Although apparently discrepant with our findings, Capes et al. (2012) did not monitor the kinetic development of TTX effects, suggesting that the results can be reconciled if the events they monitor occur on a time scale <1 s.

The structural basis for slow immobilization is not known. Supporting the notion that voltage sensors in K_V channels can reside stably in an inactive conformation, the crystal structure of the $K_V1.2$ K_V channel (Long et al., 2007) appears to show inactivated sensors (Lewis et al., 2008; Villalba-Galea et al., 2008). The dependence of $Na_V1.4$ SI on time and voltage suggests that slow immobilization of the four nonidentical sensors involves many conformations. For our simulations >1–160 s, linear five-state, four-transition models have proven adequate. However, continuous-time semi-Markovian modeling has also been used, rather than multi-exponential fits, to elegantly describe SI (Marom, 2009; Soudry and Meir, 2010), and a power law with a continuum shift of the time constant value may represent more accurately both the experimental observations and the structural basis for slow voltage-sensor transitions.

Here, we demonstrate correlation of voltage-sensor immobilization and SI, highlighting the close relationship of DI and DII with development of SI and DIII with recovery from SI. DIII appears to reflect the onset of SI but tracks it with less fidelity than DI and DII. We hypothesize that these associations are causal. In our companion paper (Silva and Goldstein 2013), we present further evidence for direct linkage of slow changes in the mobility of these voltage sensors and the onset of SI and the recovery from SI through study of a point mutation in $Na_V1.4$ that is linked to hyperkalemic periodic paralysis and impedes SI.

TABLE 5

Model parameters

Channel domain	Transition	Forward rate	Reverse rate	Reverse rate
		a	a	b
DI	A↔I1	1.74E-04	2.99E-04	5.17E+02
	I1↔I2	1.55E-05	1.55E-05	4.34E+01
	I2↔I3	1.12E-06	9.57E-03	2.04E+01
DII	A↔I1	1.42E-04	1.78E-04	3.14E+02
	I1↔I2	9.30E-06	9.10E-06	2.23E+01
	I2↔I3	9.31E-04	2.48E-04	1.08E+02
DIII	A↔I1	1.78E-04	3.34E-04	not req.
	I1↔I2	5.35E-05	3.08E-05	not req.
	I2↔I3	1.81E-07	3.64E-03	not req.
DIV	A↔I1	2.31E-04	5.04E-04	not req.
	I1↔I2	4.29E-04	6.38E-03	not req.
	I2↔I3	6.52E-04	3.57E-05	not req.

The discrete-state Markov models used to reproduce experimental data shown in Fig. 8 are parameterized with standard rate transitions: $a*\exp(-V_m/b)$. The second parameter, b, which confers voltage dependence to the rate, is only required for DI and DII sensor immobilization. Parameters for the forward and reverse rate transitions between states A and I_1, states I_1 and I_2, and states I_2 and I_3 for each of the voltage-sensor domains.

The authors are grateful to F. Bezanilla, A. Correa, D. Hanck, R. Goldstein, and S. Marom for materials and intellectual gifts during the performance of this work.

This work is supported by the National Institutes of Health (grants 5T32HL007237 and RO1NS058505 to S.A.N. Goldstein) and a Burroughs Wellcome Fund Career Award at the Scientific Interface (to J.R. Silva).

Kenton J. Swartz served as editor.

Submitted: 8 October 2012
Accepted: 11 January 2013

REFERENCES

Balser, J.R., H.B. Nuss, N. Chiamvimonvat, M.T. Pérez-García, E. Marban, and G.F. Tomaselli. 1996. External pore residue mediates slow inactivation in mu 1 rat skeletal muscle sodium channels. *J. Physiol.* 494:431–442.

Bendahhou, S., T.R. Cummins, R.W. Kula, Y.H. Fu, and L.J. Ptácek. 2002. Impairment of slow inactivation as a common mechanism for periodic paralysis in DIIS4-S5. *Neurology.* 58:1266–1272. http://dx.doi.org/10.1212/WNL.58.8.1266

Capes, D.L., M. Arcisio-Miranda, B.W. Jarecki, R.J. French, and B. Chanda. 2012. Gating transitions in the selectivity filter region of a sodium channel are coupled to the domain IV voltage sensor. *Proc. Natl. Acad. Sci. USA.* 109:2648–2653. http://dx.doi.org/10.1073/pnas.1115575109

Catterall, W.A., A.L. Goldin, and S.G. Waxman. 2005. International Union of Pharmacology. XLVII. Nomenclature and structure-function relationships of voltage-gated sodium channels. *Pharmacol. Rev.* 57:397–409. http://dx.doi.org/10.1124/pr.57.4.4

Cha, A., P.C. Ruben, A.L. George Jr., E. Fujimoto, and F. Bezanilla. 1999. Voltage sensors in domains III and IV, but not I and II, are immobilized by Na+ channel fast inactivation. *Neuron.* 22:73–87. http://dx.doi.org/10.1016/S0896-6273(00)80680-7

Chanda, B., and F. Bezanilla. 2002. Tracking voltage-dependent conformational changes in skeletal muscle sodium channel during activation. *J. Gen. Physiol.* 120:629–645. http://dx.doi.org/10.1085/jgp.20028679

Chanda, B., O.K. Asamoah, and F. Bezanilla. 2004. Coupling interactions between voltage sensors of the sodium channel as revealed by site-specific measurements. *J. Gen. Physiol.* 123:217–230. http://dx.doi.org/10.1085/jgp.200308971

Cummins, T.R., J. Zhou, F.J. Sigworth, C. Ukomadu, M. Stephan, L.J. Ptácek, and W.S. Agnew. 1993. Functional consequences of a Na+ channel mutation causing hyperkalemic periodic paralysis. *Neuron.* 10:667–678. http://dx.doi.org/10.1016/0896-6273(93)90168-Q

Featherstone, D.E., J.E. Richmond, and P.C. Ruben. 1996. Interaction between fast and slow inactivation in Skm1 sodium channels. *Biophys. J.* 71:3098–3109. http://dx.doi.org/10.1016/S0006-3495(96)79504-8

Gagnon, D.G., and F. Bezanilla. 2010. The contribution of individual subunits to the coupling of the voltage sensor to pore opening in Shaker K channels: Effect of ILT mutations in heterotetramers. *J. Gen. Physiol.* 136:555–568. http://dx.doi.org/10.1085/jgp.201010487

Hayward, L.J., R.H. Brown Jr., and S.C. Cannon. 1997. Slow inactivation differs among mutant Na channels associated with myotonia and periodic paralysis. *Biophys. J.* 72:1204–1219. http://dx.doi.org/10.1016/S0006-3495(97)78768-X

Hayward, L.J., G.M. Sandoval, and S.C. Cannon. 1999. Defective slow inactivation of sodium channels contributes to familial periodic paralysis. *Neurology.* 52:1447–1453. http://dx.doi.org/10.1212/WNL.52.7.1447

Horn, R., S. Ding, and H.J. Gruber. 2000. Immobilizing the moving parts of voltage-gated ion channels. *J. Gen. Physiol.* 116:461–476. http://dx.doi.org/10.1085/jgp.116.3.461

Lewis, A., V. Jogini, L. Blachowicz, M. Lainé, and B. Roux. 2008. Atomic constraints between the voltage sensor and the pore domain in a voltage-gated K^+ channel of known structure. *J. Gen. Physiol.* 131:549–561. http://dx.doi.org/10.1085/jgp.200809962

Long, S.B., X. Tao, E.B. Campbell, and R. MacKinnon. 2007. Atomic structure of a voltage-dependent K+ channel in a lipid membrane-like environment. *Nature.* 450:376–382. http://dx.doi.org/10.1038/nature06265

Lönnendonker, U. 1989. Use-dependent block of sodium channels in frog myelinated nerve by tetrodotoxin and saxitoxin at negative holding potentials. *Biochim. Biophys. Acta.* 985:153–160. http://dx.doi.org/10.1016/0005-2736(89)90360-X

Mannuzzu, L.M., M.M. Moronne, and E.Y. Isacoff. 1996. Direct physical measure of conformational rearrangement underlying potassium channel gating. *Science.* 271:213–216. http://dx.doi.org/10.1126/science.271.5246.213

Marom, S. 2009. Adaptive transition rates in excitable membranes. *Front Comput Neurosci.* 3:2.

McNulty, M.M., J.W. Kyle, G.M. Lipkind, and D.A. Hanck. 2006. An inner pore residue (Asn406) in the Nav1.5 channel controls slow inactivation and enhances mibefradil block to T-type Ca2+ channel levels. *Mol. Pharmacol.* 70:1514–1523. http://dx.doi.org/10.1124/mol.106.027177

Melamed-Frank, M., and S. Marom. 1999. A global defect in scaling relationship between electrical activity and availability of muscle sodium channels in hyperkalemic periodic paralysis. *Pflugers Arch.* 438:213–217. http://dx.doi.org/10.1007/s004240050900

Sandtner, W., J. Szendroedi, T. Zarrabi, E. Zebedin, K. Hilber, I. Glaaser, H.A. Fozzard, S.C. Dudley, and H. Todt. 2004. Lidocaine: a foot in the door of the inner vestibule prevents ultra-slow inactivation of a voltage-gated sodium channel. *Mol. Pharmacol.* 66:648–657.

Shaw, R.M., and Y. Rudy. 1997. Ionic mechanisms of propagation in cardiac tissue. Roles of the sodium and L-type calcium currents during reduced excitability and decreased gap junction coupling. *Circ. Res.* 81:727–741. http://dx.doi.org/10.1161/01.RES.81.5.727

Sheets, M.F., J.W. Kyle, and D.A. Hanck. 2000. The role of the putative inactivation lid in sodium channel gating current immobilization. *J. Gen. Physiol.* 115:609–620. http://dx.doi.org/10.1085/jgp.115.5.609

Silva, J.R., and S.A.N. Goldstein. 2013. Voltage-sensor movements describe slow inactivation of voltage-gated sodium channels II: A periodic paralysis mutation in $Na_V1.4$ (L689I). *J. Gen. Physiol.* 141:323–334.

Sokolov, S., R.L. Kraus, T. Scheuer, and W.A. Catterall. 2008. Inhibition of sodium channel gating by trapping the domain II voltage sensor with protoxin II. *Mol. Pharmacol.* 73:1020–1028. http://dx.doi.org/10.1124/mol.107.041046

Soudry, D., and R. Meir. 2010. History-dependent dynamics in a generic model of ion channels—an analytic study. *Front Comput Neurosci.* 4:12.

Stefani, E., L. Toro, E. Perozo, and F. Bezanilla. 1994. Gating of Shaker K+ channels: I. Ionic and gating currents. *Biophys. J.* 66:996–1010. http://dx.doi.org/10.1016/S0006-3495(94)80881-1

Szendroedi, J., W. Sandtner, T. Zarrabi, E. Zebedin, K. Hilber, S.C. Dudley Jr., H.A. Fozzard, and H. Todt. 2007. Speeding the recovery from ultraslow inactivation of voltage-gated Na+ channels by metal ion binding to the selectivity filter:

a foot-on-the-door? *Biophys. J.* 93:4209–4224. http://dx.doi.org/10.1529/biophysj.107.104794

Toib, A., V. Lyakhov, and S. Marom. 1998. Interaction between duration of activity and time course of recovery from slow inactivation in mammalian brain Na+ channels. *J. Neurosci.* 18: 1893–1903.

Townsend, C., and R. Horn. 1997. Effect of alkali metal cations on slow inactivation of cardiac Na^+ channels. *J. Gen. Physiol.* 110:23–33. http://dx.doi.org/10.1085/jgp.110.1.23

Vilin, Y.Y., and P.C. Ruben. 2001. Slow inactivation in voltage-gated sodium channels: molecular substrates and contributions to channelopathies. *Cell Biochem. Biophys.* 35:171–190. http://dx.doi.org/10.1385/CBB:35:2:171

Vilin, Y.Y., N. Makita, A.L. George Jr., and P.C. Ruben. 1999. Structural determinants of slow inactivation in human cardiac and skeletal muscle sodium channels. *Biophys. J.* 77:1384–1393. http://dx.doi.org/10.1016/S0006-3495(99)76987-0

Villalba-Galea, C.A., W. Sandtner, D.M. Starace, and F. Bezanilla. 2008. S4-based voltage sensors have three major conformations. *Proc. Natl. Acad. Sci. USA.* 105:17600–17607. http://dx.doi.org/10.1073/pnas.0807387105

Webb, J., and S.C. Cannon. 2008. Cold-induced defects of sodium channel gating in atypical periodic paralysis plus myotonia. *Neurology.* 70:755–761. http://dx.doi.org/10.1212/01.wnl.0000265397.70057.d8

Xiong, W., R.A. Li, Y. Tian, and G.F. Tomaselli. 2003. Molecular motions of the outer ring of charge of the sodium channel: Do they couple to slow inactivation? *J. Gen. Physiol.* 122:323–332. http://dx.doi.org/10.1085/jgp.200308881

Xiong, W., Y.Z. Farukhi, Y. Tian, D. Disilvestre, R.A. Li, and G.F. Tomaselli. 2006. A conserved ring of charge in mammalian Na+ channels: a molecular regulator of the outer pore conformation during slow inactivation. *J. Physiol.* 576:739–754. http://dx.doi.org/10.1113/jphysiol.2006.115105